IOP PUBLISHING JOURNAL OF PHYSICS D: APPLIED PHYSICS
J. Phys. D: Appl. Phys. **40** (2007) 5847–5853 doi:10.1088/0022-3727/40/19/008

Modified spontaneous emission of silicon nanocrystals embedded in artificial opals

Petr Janda[1], Jan Valenta[1], Jean-Luc Rehspringer[2], Rodrigue R Mafouana[2], Jan Linnros[3] and Robert G Elliman[4]

[1] Department of Chemical Physics and Optics, Faculty of Mathematics and Physics, Charles University, Ke Karlovu 3, 121 16 Prague 2, Czechia
[2] Institut de Physique et Chimie des Matériaux de Strasbourg, GMI et GONLO, UMR46 CNRS-ULP-ECPM, 23, rue du Loess, F-67037 Strasbourg, France
[3] Laboratory of Material and Semiconductor Physics, Royal Institute of Technology, Electrum 229, 164 21 Kista-Stockholm, Sweden
[4] Electronic Materials Engineering Department, Research School of Physical Sciences and Engineering, Australian National University, Canberra, ACT 0200, Australia

E-mail: jan.valenta@mff.cuni.cz

Received 4 June 2007, in final form 8 August 2007
Published 21 September 2007
Online at stacks.iop.org/JPhysD/40/5847

Abstract

Si nanocrystals (NCs) were embedded in synthetic silica opals by means of Si-ion implantation or opal impregnation with porous-Si suspensions. In both types of sample photoluminescence (PL) is strongly Bragg-reflection attenuated (up to 75%) at the frequency of the opal stop-band in a direction perpendicular to the (1 1 1) face of the perfect hcp opal structure. Time-resolved PL shows a rich distribution of decay rates, which contains both shorter and longer decay components compared with the ordinary stretched exponential decay of Si NCs. This effect reflects changes in the spontaneous emission rate of Si NCs due to variations in the local density of states of real opal containing defects.

1. Introduction

Silicon nanostructures are promising materials for realizing all-silicon optoelectronics. Light emission from bulk silicon is very inefficient due to its indirect band-gap structure and the dominance of non-radiative recombination. In contrast, nanocrystalline silicon shows much stronger photoluminescence (PL) with quantum efficiency of the order of several per cent [1]. However, the performance of Si-based light-emitting devices is limited by a relatively low emission rate and a broad emission spectrum. One possible way to manipulate the emission rate, wavelength and direction is the inclusion of Si nanocrystals (NCs) within photonic structures. For example, silicon NCs can form active planar waveguides that exhibit significant PL narrowing, polarization and directionality [2]. They may also be coupled to a spherical micro-cavity and show whispering gallery modes in PL spectra [3, 4].

The suppression of spontaneous emission by photonic band-gap structures was proposed in the seminal paper by Jablonovitch in 1987 [5] and is probably most clearly demonstrated for PL from a GaInAsP quantum well in a 2D photonic-crystal slab (five times reduction of the PL emission rate in the near-infrared spectral region) [6]. Throughout the past decade artificial opal has been used to demonstrate the influence of photonic structure on the luminescence of dye molecules or NCs in the visible spectral range [7]. Artificial opals are prepared from sub-micrometre beads of silica, polystyrene, etc, which are organized into a stochastic mixture of hcp and fcc structures [8]. However, such a material exhibits only optical stop-bands (not a complete photonic band-gap) due to the fact that the refractive index contrast between the beads and voids is low. This problem can be overcome by using inverted opals that are formed by filling the opal pores with a higher index material (silicon [9], TiO_2 [10], etc) and removing initial (template) beads. This can be used to increase the refractive index contrast and thereby produce a larger modification of the density of photonic states. Several attempts to fill the opal voids with semiconductor NCs have been undertaken and their modified emission reported [11–15].

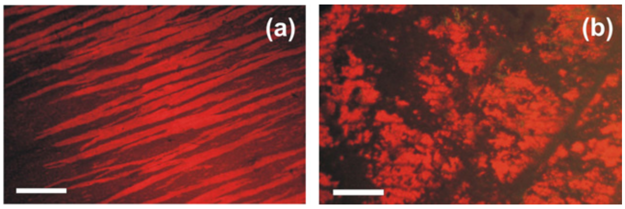

Figure 1. Colour reflection micro-photographs of two opal samples used in this study. The white bars are 0.2 mm long. Regions with low omnispectral diffuse reflection and strong red reflection due to the stop-band are clearly resolved.

In this paper we report on the fabrication of Si NCs in silica artificial opals by means of Si-ion implantation or opal impregnation with porous-Si (P-Si) colloidal suspensions. PL spectra of Si NCs at the stop-band frequency are shown to be largely attenuated by Bragg reflection. PL decay rates show new slow and fast components due to variations in the local density of photonic states in the opal. Micro-PL imaging also highlights interesting aspects associated with light localization by defects.

2. Sample preparation and experimental set-up

Silica microspheres were prepared following the modified Stöber–Finck process that has been shown to result in particle size dispersion better than about 2%. Large synthetic opals were prepared using electro-sedimentation from the colloidal solution of silica spheres. The sedimentation lasts for approximately 4 days under static electric fields of 0.2 V cm^{-1} applied between a platinum grid and a mercury layer. Self-supporting bulk opals were obtained by partial sintering of the silica particles at 950 °C for 2 h (figure 1). The mean diameter of the silica spheres used in this study was about 300 nm (figure 2(*a*)). Electron microscope and AFM images reveal an fcc structure of opal with a (1 1 1) plane on the surface. Figure 2(*b*) shows a Fourier transform of the image in figure 2(*a*) which highlights the hexagonal structure of the opal and shows a layer periodicity of 288 nm and a mean bead size of 333 nm.

Si NCs were introduced into the opal in two ways.

- Si$^-$ ion implantation (energy of 100 keV and dose of 0.5×10^{17} cm^{-2}) followed by annealing at 1100 °C for 1 h in nitrogen. This procedure formed Si nanocrystals inside the SiO$_2$ spheres. A transport of ions in matter (TRIM) calculation [16] of the implantation profile for 100 keV Si-ions into quartz reveals a mean projected range of 150 nm. A simple numerical calculation gives an estimation of the excess Si concentration in the case of an opal structure (neglecting the curvature of the silica spheres) showing that 66%, 29% and 5% of the ions are stopped in the first, second and third layers of silica spheres, respectively (implanting the (1 1 1) plane of a perfect opal fcc crystal). Under such implantation conditions the deformation of silica spheres is negligible.
- Luminescing Si NCs were formed by conventional electrochemical etching of Si wafers (⟨1 0 0⟩ p-type, $\rho \sim 0.1\ \Omega$ cm) in a HF-ethanol (1 : 2.5) solution. The etching current density was kept relatively low (1.6 mA cm^{-2}) in order to obtain higher porosity and, consequently, resulting in a low mean size of Si-nc (the PL band peak is around 680 nm). P-Si powder (i.e. grains of interconnected oxidized Si NCs) was then obtained by mechanical pulverization (scratching with a blade) of the P-Si film from the silicon substrate. A colloidal suspension was prepared by pouring ethanol onto the P-Si powder and mixing it in an ultrasonic bath. The suspension was then sedimented for several days and the supernatant component extracted and dispensed onto the opal surface. The opal surface was subsequently flushed with high-pressure-filtered air to remove any residual P-Si particles. The size distribution of impregnated particles is broad ranging from tens to hundreds of nanometres.

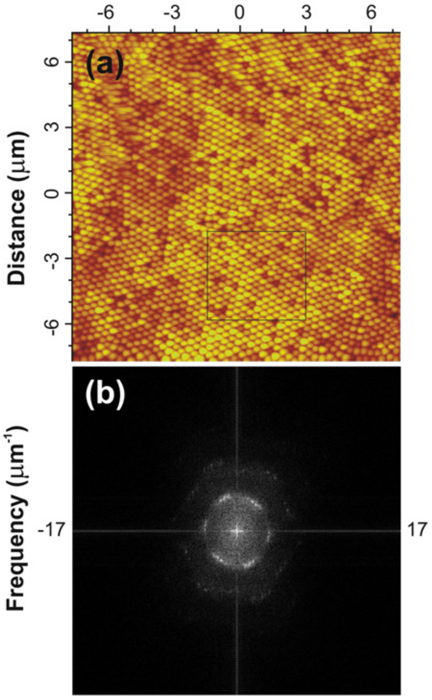

Figure 2. (*a*) Atomic force microscope view of the 15 × 15 μm^2 surface of one opal sample. (*b*) Two-dimensional spatial Fourier transform of the upper figure clearly showing the hexagonal structure of the opal. The periodicity and particle size is 288 nm and 333 nm, respectively.

PL and reflection spectra were measured using micro-spectroscopy set-ups based on imaging spectrographs (Horiba Jobin Yvon Triax 190 or 320) connected to conventional far-field microscopes. A liquid nitrogen (LN)-cooled CCD camera (Hamamatsu C4880) or amplified thermoelectrically (TE)-cooled camera (Princeton Instruments PI-max) was used for the detection of images and spectra. The set-up enables controlled measurement of reflection or PL spectra from any spot on the sample with resolution down to the diffraction limit (i.e. roughly 500 nm for visible wavelengths). All presented measurements were done in the direction (i.e. the optical axis of a microscope lens) perpendicular to the sample surface. The UV-line of a cw He–Cd laser (325 nm) was employed to excite the PL (in the grazing incidence to the observed sample plane, excitation intensity up to 0.5 W cm^{-2}) and a halogen lamp (focused and collected by the microscope objective lens) was used for reflection measurement. Time-resolved PL was

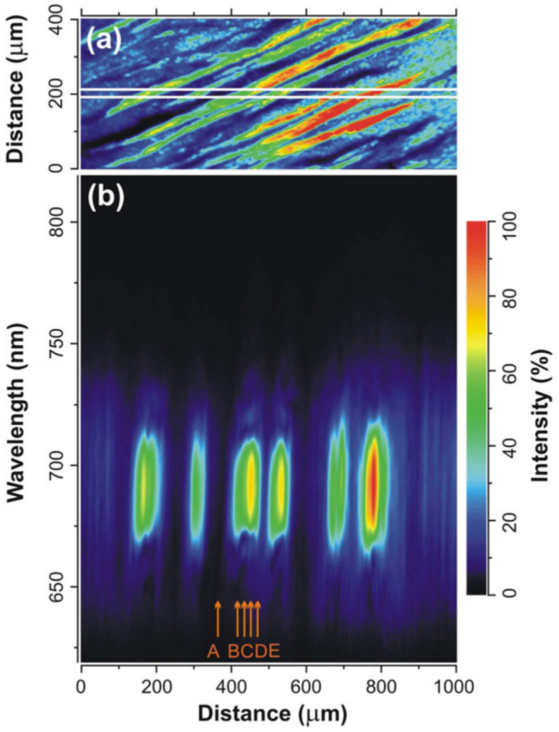

Figure 3. (*a*) Microscopic reflection image of the opal (objective lens 5×, NA = 0.13) in false colours (the colour scale is on the right-hand side of the figure). (*b*) Reflection spectral image of the slit indicated on the upper panel by white lines. Arrows show positions of spectra plotted in figure 4(*a*).

excited with an optical parametric oscillator (tuned to 420 nm, pulse duration around 5 ns and excitation density on the sample of about 70 kW cm^{-2}) pumped with a pulsed Nd : YAG laser (Ekspla NL303 and PG122) and detected with a PI-max camera (Princeton Instruments). Reflection micro-photographs were taken with a digital camera Olympus Camedia C5060wz and a micro-adapter C3040-ADUS.

3. Experimental results and discussion

3.1. Reflection spectra

Reflection micro-imaging and spectroscopy of opals reveal large variations of reflection intensity due to the existence of domains with various crystalline qualities (figures 1 and 3(*a*)). Regions with high reflection in directions perpendicular to the surface have a perfect stop-band around 690 nm (compare figures 3(*b*) and 4). The relative band width $\Delta\lambda/\lambda_C$ is about 0.055 (figure 4(*b*)) consistent with a high-quality photonic-crystal structure. Due to the directionality of the stop-band reflection the best reflection spectra are detected with low numerical aperture lenses on a well-oriented opal surface (figure 4(*b*)).

The distance that light can penetrate into a photonic crystal (in the direction and frequency of the stop-band) is characterized by the Bragg attenuation length $l_B = 2d/[\pi \cdot (\Delta\lambda/\lambda_C)]$, where d is the distance of reflecting planes (in the present case the period of (1 1 1) planes is about 288 nm) [17]. For the ordered areas of the opals we therefore obtain Bragg lengths as short as 3.3 μm (i.e. less than 12 planes).

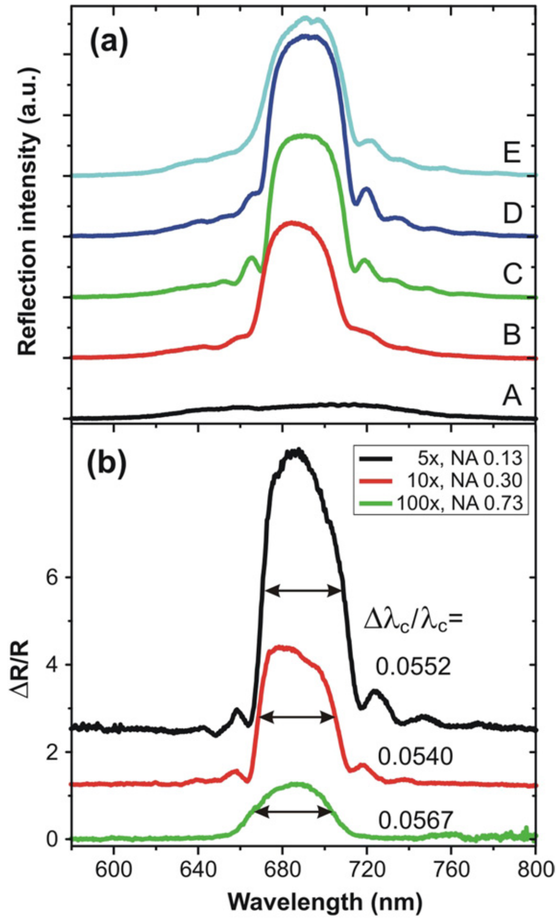

Figure 4. (*a*) Reflection spectra extracted from different positions in figure 3(*b*). (*b*) Relative reflection changes between an ordered and a disordered place of the opal sample observed with lenses of different numerical aperture and magnification. Relative band-widths $\Delta\lambda/\lambda_C$ are indicated.

Implantation or impregnation of opals with Si NCs does not change the position or width of the stop-band significantly. The variations within a sample (due to varying crystalline qualities) are much more significant.

3.2. PL of undoped opals

Under UV-light excitation the opals without Si NCs show a weak bluish PL emission (possibly due to the oxygen-deficiency centres in silica [18]). In figure 5(*a*) we compare these PL spectra in places with excellent and poor stop-band reflection. At the position of the perfect stop-band the PL intensity is reduced by up to 70% (see figure 5(*b*)). The full-width at half-maximum (FWHM) is almost equal (more precisely it is about 5% narrower) to the reflection band at the same position on the sample.

This attenuation is comparable to the results on emission changes in opals published in the literature. The fact that the attenuation is never complete is explained by Schriemer *et al* [19] by a simple model taking into account diffuse scattering of light by intrinsic defects. The scattering by opal defects limits the mean free path l of light propagation to about 15 μm in the best reported opals. Light originating from shallower layers than l_B is hardly Bragg-attenuated ,while light coming

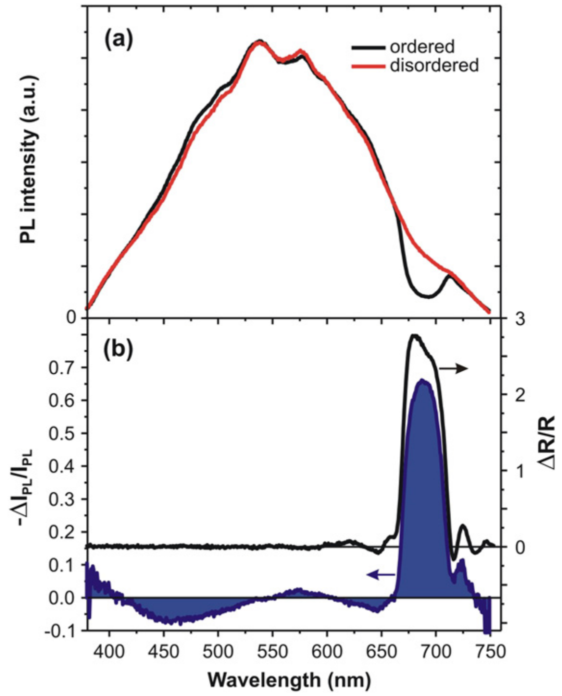

Figure 5. (*a*) PL spectra of the as-prepared opal without silicon NCs. The black and red lines represent spectra from an ordered and a disordered area of the opal, respectively. (*b*) Relative decrease of PL (blue area) calculated from the upper panel compared with relative reflection difference on the ordered and the disordered opal spots (black line).

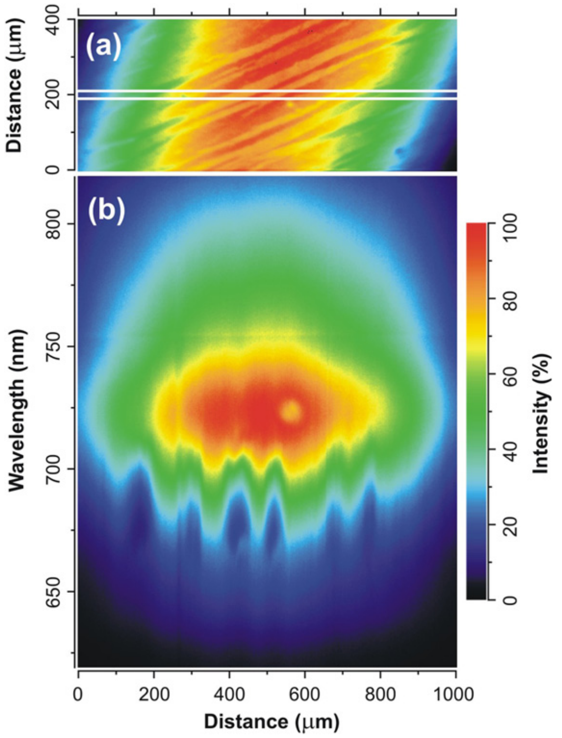

Figure 6. (*a*) Microscopic PL image of the opal (the same area as in figure 3(*a*)) in false colours (the colour scale is on the right-hand side of the figure). (*b*) PL spectral image of the slit area indicated on the upper panel by white lines.

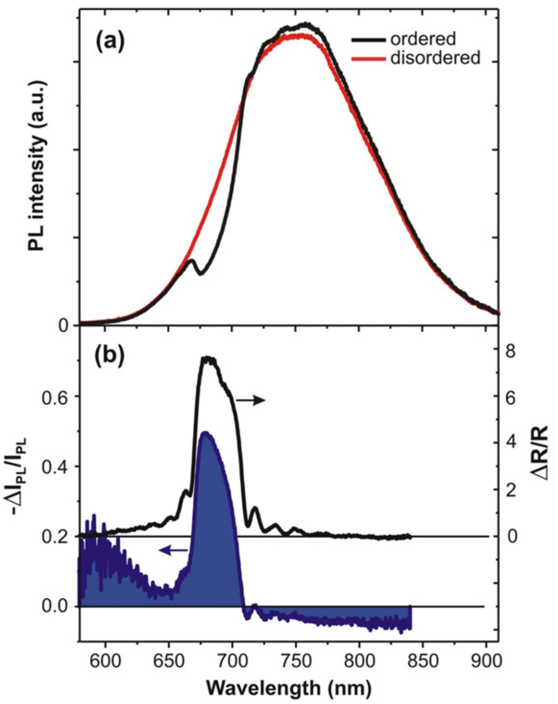

Figure 7. (*a*) PL spectra of the Si-ion-implanted opal. The black and red lines represent spectra from ordered and disordered areas, respectively. (*b*) Relative decrease of PL calculated from the upper panel (blue area) compared with relative reflection difference on the same opal spots (black line).

from deeper layers (but smaller than l) reveals the stop-band. The attenuation A of emission in the stop band is related to the mean free path and the Bragg length through the equation $A = 1 - (l_B/l)$. The value of A is usually between 0.5 and 0.8. [17]. For undoped opal (figure 5(*b*)) we observe $A \sim 0.7$, suggesting that l should be about 11 μm.

3.3. *PL of implanted opals*

Implanted regions of opal show red PL with a single wide band typical of Si nanocrystalline materials. Modifications of the PL spectra due to the opal stop-band were partially described in our previous paper [11]. In figure 6(*a*) we show a micro-PL image of the same area as shown in the reflection image of figure 3(*a*). The corresponding PL spectral image is shown in figure 6(*b*) and the PL spectra in figure 7. The PL reduction in the stop-band position is up to 50%. The effect is less pronounced than the PL reduction in bare opal, because implantation by Si-ions at 100 keV affects only the layers close to the surface. A relative decrease in the PL intensity calculated from the upper panel (blue area) is compared with the relative reflection difference on the same opal spots (black line) in figure 7(*b*).

3.4. *PL of impregnated opals*

The opal impregnated with the P-Si colloid also reveals a typical decrease in PL at the stop-band (figure 8(*a*)). Here the position of the stop-band happens to be near the PL maximum (~680 nm) and the PL depression is observed to be more than 70% (figure 8(*b*)). We note that the FWHM of the stop-band is

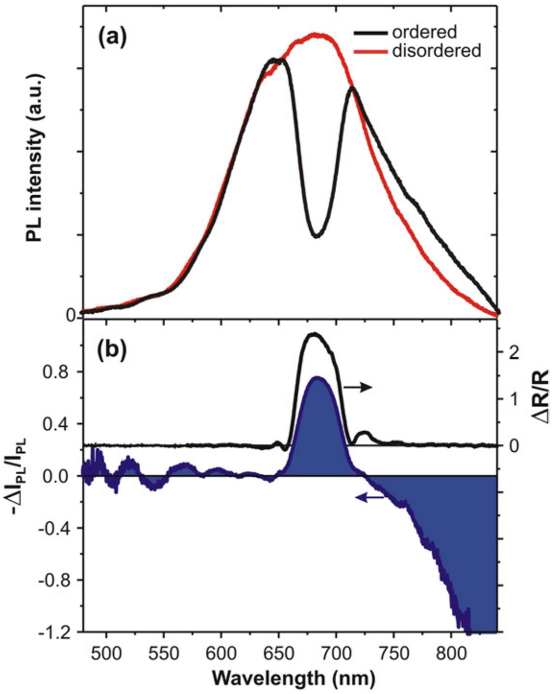

Figure 8. (*a*) PL spectra of the opal impregnated with the P-Si colloidal suspension. The black and red lines represent spectra from an ordered and disordered area, respectively. (*b*) Relative decrease of PL calculated from the upper panel (blue area) compared with relative reflection difference on the same opal spots (black line).

equal to the FWHM of the PL dip (38 nm, 100 meV) and that this value is also comparable to the 120 meV homogeneous width of the PL spectra of single Si quantum dots [20]. (The FWHM of the whole PL band is about 374 meV, i.e. three times wider than the homogeneous linewidth.)

At the long-wavelength side of the PL spectrum we observe increased emission. Although the absolute comparison of the PL intensity from different places of opal has limited precision due to non-perfect morphology of the opal, in this case the effect is observed systematically and is strong enough to be considered as real. Possible explanations for this PL enhancement based on the formation of standing waves at the edges of stop gaps [21] or the escape of diffuse light [17] predict enhancement of emission at the short-wavelength side of the spectrum (at higher frequency than the stop-band). Therefore we can rule them out. We therefore propose that reabsorption of PL from smaller Si NCs by larger NCs and their reemission is responsible for the apparent PL increase at the long-wavelength edge of the spectrum.

The PL decay of P-Si grains in disordered areas of the opal shows (figure 9) a typical stretched exponential decay $\sim\exp[-(t/\tau)^{\beta}]$ ($\tau = 33.2$ ms and $\beta = 0.765$), while the perfectly ordered region of opal gives a decay with a significantly wider distribution of decay rates. There are always both shorter and longer kinetic components and the whole PL decay curve cannot be fitted with the above-described stretched exponential function. Here we fitted the decay curve with two exponential decays ($\tau = 1.5\ \mu$s and 2.1 ms) added to a stretched exponential identical to that used above. We have to note that such a combination of functions applied to fit the decay data is obviously not the only choice, but it was selected in order to highlight the difference between decay curves in ordered and disordered regions.

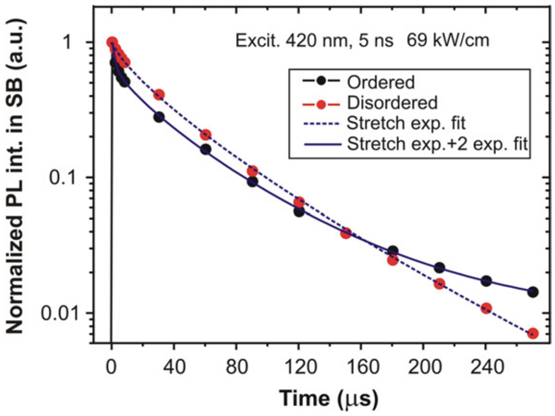

Figure 9. Si NC PL decay measured at the wavelength of the stop-band in ordered (black dots) and disordered (red dots) areas (the signal was collected from well selected $80 \times 60\ \mu\text{m}^2$ areas of the opal). The decay in disordered opal can be fitted with a stretch exponential function (blue dashed line) with parameters $\tau = 33.2\ \mu$s and $\beta = 0.765$, while in the ordered opal (continuous blue line) we had to add a fast exponential decay ($\tau = 1.5\ \mu$s, amplitude 0.29) and a slow exponential component ($\tau = 2.1$ ms, amplitude 0.011). The curves are normalized to the same peak intensity.

Since we are comparing decay rates from chemically identical regions of the impregnated opal which differ only in their structural perfection, the broader distribution of decay rates is most likely due to variations in the local density of photonic states. A low density of photonic states at the stop-band frequency and direction decreases the probability of spontaneous emission (PL) while defects in the structure localize the photonic states (such as defects inside band-gaps of semiconductors) and increase the rate of emission [22].

3.5. *Local variations of PL intensity*

In order to confirm that local variations in the PL intensity are due to structural variations we studied micro-PL images with high magnification. For this experiment we used only implanted opals where the distribution of Si NCs is very homogeneous (in contrast to impregnated opals with P-Si colloids that do not necessarily provide an equal distribution of NCs). In figure 10 we show high magnification images (objective lens 100×, NA = 0.73) of reflection (*a*) and PL (*b*) on the implanted opal (area with excellent stop-band in average reflection view). Panels (*c*) and (*d*) plot the respective intensity profiles (average intensity being normalized to unity). One can see that intensity variations are mainly within 20% (and sometimes 40%) of the average value. In some locations we observe correlations between decreased reflection and increased PL. We speculate that this is due to structural defects (e.g. several missing opal beads). In figure 11 we show one such place which has the shape of a ring (the micro-PL image in the inset of figure 11). The PL intensity in the ring is about 20% higher than out of the ring (figure 11). The stop-band signature is missing in the PL spectrum as we use the objective with high NA that mixes signal leaving the sample within a wide solid angle.

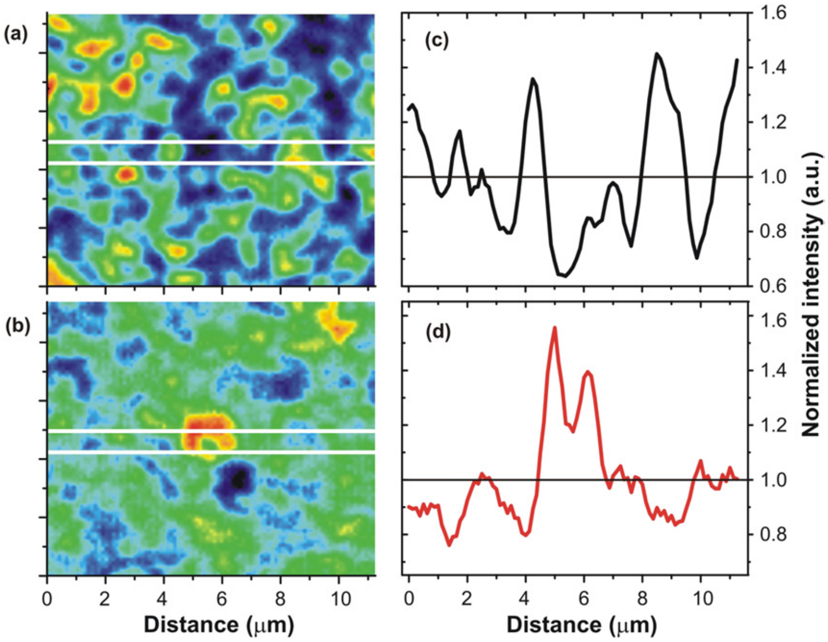

Figure 10. High magnification images (objective lens 100×, NA = 0.73, false colour represents intensities) of reflection (*a*) and PL (*b*) on the implanted opal (area with excellent stop-band seen in a wider reflection view). Panels (*c*) and (*d*) plot intensity profiles from areas in panels (*a*) and (*b*), respectively. (Average intensity is normalized to unity.)

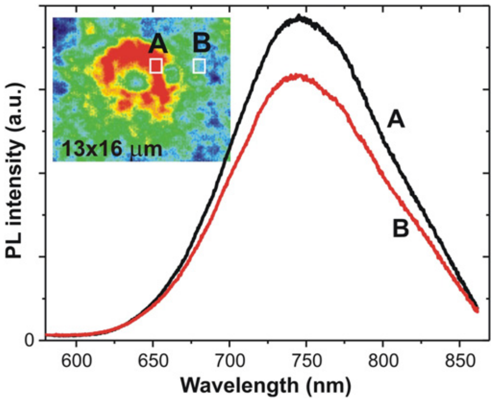

Figure 11. PL spectra measured in (A—black curve) and out (B—red curve) of the light circle. The PL image with detected areas is shown in the inset. (Objective lens 100×, NA = 0.73.)

A deeper understanding of the processes responsible for variations in the spontaneous emission rate and variations of the PL intensity is the subject of further study.

4. Conclusions

We have prepared light-emitting Si NCs inside artificial opals by means of Si-ion implantation or impregnation with P-Si suspensions. In both cases we observed significant changes in Si-NC luminescence at the opal stop-band frequency in directions perpendicular to the opal (1 1 1) surface. The luminescence intensity was shown to be reduced by as much as 75% at the stop-band mainly due to Bragg-reflection attenuation. There is also a signature of enhanced PL at the red-edge of PL spectra of Si NCs impregnated in the perfect opal structure which is interpreted as absorption and reemission of PL within the inhomogeneously broadened PL band. PL decay times for Si NCs embedded in a well-ordered opal were also shown to exhibit new slower as well as faster components compared with the standard stretched exponential decay of Si NCs. These observations demonstrate that photonic crystals can have a significant effect on the broadband emission of silicon NCs and suggest that more refined photonic structures could have potential application for novel Si-based optoelectronic devices and structures.

Acknowledgments

This work was supported by the Czech Ministry of education, youth and sports through the research centre LC510 and the research plan MSM0021620835 and the Project 202/07/0818 of the Grant Agency of the Czech Republic. Partial support from the Australian Research Council and the Royal Swedish Academy of Sciences is also acknowledged.

References

[1] Ossicini S, Pavesi L, and Priolo F 2003 *Light Emitting Silicon for Microphotonics* (Berlin: Springer)
[2] Pelant I, Ostatnicky T, Valenta J, Luterova K, Skopalova E, Mates T and Elliman R G 2006 *Appl. Phys.* B **83** 87
[3] Meldrum A, Hryciw A, Buchanan K S, Beltaos A M, Glover M, Ryan C A and Veinot J G C 2005 *Opt. Mater.* **27** 812
[4] Beltaos A M and Meldrum A 2007 *J. Luminesc.* **126** 607
[5] Jablonovitch E 1987 *Phys. Rev. Lett.* **58** 2059
[6] Fujita M, Takahashi S, Tanaka Y, Asano T and Noda S 2005 *Science* **308** 1298
[7] Lopez C 2003 *Adv. Mater.* **15** 1679
[8] Bogomolov V N, Gaponenko S V, Germanenko I N, Kapitonov A M, Petrov E P, Gaponenko N V, Prokofjev A V, Ponyavina A N, Silvanovich N I and Samoilovich S M 1997 *Phys. Rev.* E **55** 7619

[9] Díaz-Guerra C, Piqueras J, Golubev V G, Kurdyukov D A and Pevtsov A B 2001 *J. Appl. Phys.* **90** 3659

[10] Koederink A F, Bechger L, Schriemer H P, Lagendijk A and Vos W L 2001 *Phys. Rev. Lett.* **88** 143903

[11] Valenta J, Linnros J, Juhasz R, Rehspringer J-L, Huber F, Hirlimann Ch, Cheylan S and Elliman R G 2003 *J. Appl. Phys.* **93** 4471

[12] Gaponenko S V, Kapitonov A M, Bogomolov V N, Prokofiev A V, Eychmüller A and Rogach A L 1998 *JETP Lett.* **68** 142

[13] Romanov S G, Chigrin D N, Solovyev V G, Maka T, Gaponik N, Eychmüller A, Rogach A L and Sotomayor Torres C M 2003 *Phys. Status. Solidi.* a **197** 662

[14] Vlasov Yu A, Deutch M and Norris D J 2000 *Appl. Phys. Lett.* **76** 1627

[15] Barth M, Gruber A and Cichos F 2005 *Phys. Rev.* B **72** 085129

[16] Ziegler J F, Biersack J P and Littmark U 1996 *The Stopping and Range of Ions in Solids* (New York: Pergamon)

[17] Bechger L, Lodahl P and Vos W L 2005 *J. Phys. Chem.* B **109** 9980

[18] Skuja L 1998 *J. Non-Cryst. Solids* **239** 16

[19] Schriemer H P, van Driel H M, Koenderink A F and Vos W L 2000 *Phys. Rev.* A **63** 011801

[20] Valenta J, Juhasz R and Linnros J 2002 *Appl. Phys. Lett.* **80** 1070

[21] Galstyan A G, Raikh M E and Vardeny Z V 2000 *Phys. Rev.* B **62** 1780

[22] Novotny L and Hecht B 2005 *Principles of Nano-Optics* (Cambridge: Cambridge University Press)